Trends in Chemical Engineering
Vol. 22, 2024

Original Article

CO_2/brine/rock interactions in the Cedar Keys-Lawson Formation under sequestration conditions

Yee Soong[1,*], Bret H. Howard[1], Igor Haljasmaa[1,2], Dustin Crandall[1], Laura E. Dalton[3], Wu Zhang[1], Ping Wang[1], Vyacheslav Romanov[1], McMahan L. Gray[1] and Fan Shi[1]

[1]National Energy Technology Laboratory (NETL), U.S. Department of Energy, 626 Cochran Mill Road, Pittsburgh, PA 15236, USA; [2]NETL Support Contractor, Leidos Inc., 626 Cochran Mill Road, Pittsburgh, PA 15236, USA; [3]Department of Civil and Environmental Engineering, Ciemas 2469, Duke University, Durham, NC 27708, USA.

ABSTRACT

Deep saline aquifers have the largest estimated capacity for CO_2 storage among many geologic storage options. Obtaining insight into possible geochemically induced changes to the host CO_2 storage rocks such as permeability and porosity will enable us to gain knowledge on long-term reservoir behavior under CO_2 storage conditions. An experimental study of the interaction of CO_2/brine/rock was conducted in a static system under CO_2 storage conditions. Chemical interactions in the Cedar Keys-Lawson Formation dolostone during exposure to CO_2 and brine under sequestration conditions were studied. Samples were exposed to the simulated *in-situ* reaction conditions for six, twelve, and twenty-four months. The samples were exposed to a model brine at 55 °C and CO_2 pressure of 23.8 MPa (3,500 psig). Computed tomography (CT), x-ray diffraction (XRD), scanning electron microscopy (SEM)-energy dispersive x-ray spectroscopy (EDS), brine composition, core porosity, and core permeability analyses were conducted prior to and after the exposure experiments. The core samples showed a decrease of porosity after they were exposed to CO_2-saturated brine for the period of six, twelve and twenty-four months. This observation implies that mineral precipitation could occur in the host rock thus changing its characteristics for CO_2 storage over time. The measured permeabilities for six- and twelve-month exposure samples show an increase. The CT images of the pore space clearly indicate the degree of dissolution that occurred during the six-month exposure. It is noted that the dolomite, anhydrite, and gypsum dissolution that occurred during the six-month exposure could have enhanced the connectivity between voids. This may contribute to the increase of permeability after the CO_2/brine exposure. However, the 23% decrease of permeability after the twenty-four month exposure experiment likely relates to NaCl and mineral precipitation blocking the connectivity of pores resulting in the observed decrease in permeability.

KEYWORDS: CO_2 sequestration, Cedar Keys-Lawson Formation, permeability, saline aquifer.

INTRODUCTION

Among many strategies to mitigate the effect of anthropogenic CO_2 on global climate change, carbon capture and storage (CCS) is identified as a major strategy for reducing the contribution of CO_2 from power plants and energy-intensive industries [1, 2]. In particular, CCS technologies could eliminate CO_2 emissions from stationary

*Corresponding author: yee.soong@netl.doe.gov

sources of carbon emission by separating CO_2 from flue gases, pressurizing, and transporting it *via* pipeline to underground geologic formations where it is injected into porous rock layers that are sealed by impermeable caprocks for permanent storage. CO_2 geological storage has proven to be an efficient method for reducing anthropogenic greenhouse gas emissions. Through this method, million tons of CO_2 emissions are stored globally in geological storage formations (i.e., deep saline aquifers, basaltic rocks, coal bed methane formations, tight shale formations, and depleted hydrocarbon reservoirs) [2-4]. The capacity for various CO_2 storage options depends on various factors such as the porosity, permeability, depth, pressure, temperature, and integrity of the storage formations and the caprocks. The largest estimated CO_2 storage potential was identified in saline aquifers within underground geological formations [2-4]. Deep saline aquifers have a vast capacity for storing CO_2 and are abundant worldwide. The amount of CO_2 that can be stored in the formations may comprise most of the total accumulated underground CO_2 storage capacity [3, 4]. These geological formations are typically sandstone or carbonate formations. Carbonate formations are often highly permeable and provide accommodation for a large amount of CO_2 injection compared to sandstone formations with low permeability. The cap rock, which provides a seal to trap buoyant CO_2 to prevent capillary leakage, is typically shale [3, 4].

Many studies have been conducted to investigate changes in host rock properties when exposed to CO_2 within the Mount Simon formation, the Lower Tuscaloosa formation as well as other potential CO_2 storage sites [5-18]. Studies showed that the alterations depend on the rock composition as well as the progressive dissolution of CO_2 in the brine that leads to a decrease in pH [5]. As a result, the primary expected process involves dissolution of carbonates and eventually silicates, depending on the kinetics of the individual reactions [6]. Specifically, dissolution leads to a change in porosity and permeability as well as modifications to the surface area of the reactive mineral. Furthermore, the increase of cation concentration produced by mineral dissolution can supersaturate the fluids. In this case, precipitation processes can lead to further changes of porosity and permeability.

A simulation study of potential effects of CO_2 sequestration in the Mount Simon sandstone was conducted by Liu *et al.* [8]. The study reported that a strongly acidified zone (pH 3-5) forms in the areas affected by the injected CO_2 and thus causes secondary mineral precipitation (ankerite, alunite, anhydrite, calcite, and magnesite) and dissolution of feldspars. During the injection period of 100 years, the dominant chemical reactions are dolomite dissolution and calcite, magnesite, and ankerite precipitation. These carbonate reactions resulted in a slight increase in porosity (1%). Acidification resulting from CO_2 dissolution ultimately caused dissolution of nearly all K-feldspar (21.2% by volume) near the injection well and replacement by alunite and anhydrite. A CO_2/brine/rock interaction study utilizing Mount Simon sandstone and Eau Claire shale cores collected from the FutureGen storage site (Jacksonville, Illinois) was conducted by Szecsody *et al.* [19] for a period of 1.2 years at 38 °C and CO_2 pressures up to 12.4 MPa. A significant increase in K, Mg, and SO_4^{2-} concentrations, the dissolution of hematite coating on the quartz grains, significant precipitation of NaCl, KCl, and some iron oxide particulate movement were reported by this investigation. No permeability or porosity changes were reported in this study. Soong *et al*. [20] reported that mineral dissolution/precipitation could occur under CO_2 storage conditions for cores obtained from the Mount Simon formation (Indiana). Complementary core-scale numerical simulations of the Mount Simon sandstone/CO_2-saturated brine geochemical interactions predicted dissolution of quartz and feldspar with subsequent formation of kaolinite which would result in a net decrease in permeability [21]. Tutolo *et al*. [22] conducted a study using K-feldspar-rich sandstone from the Eau Claire formation (Indiana) at 150 °C, and 20 MPa in a flow-through apparatus. Results of that study indicated dissolution of feldspar and precipitation of secondary aluminum minerals, such as boehmite. They also reported a decrease in bulk permeability and lower porosity in the

post-experiment core samples. It has been reported that the permeability of the reservoir rock is affected by the combination of dissolution and precipitation [20]. Dissolution of the small amounts of cementing minerals, such as calcite, can change the permeability significantly as also reported by Nogues *et al*. [23].

Core samples from the Mount Simon formation in Illinois were also investigated under CO_2 sequestration conditions of 85 °C and 23.8 MPa of CO_2 in the presence of brine [24]. A 12% decrease in permeability was found in the sandstone cored parallel to the bedding plane after it was exposed to CO_2-saturated brine for six months. This was probably due to mineral dissolution, migration and secondary mineral precipitation altering the sandstone pore/crack structure. For the case of the core sample taken perpendicular to the bedding plane, decreasing permeability may be linked to mineral precipitation in the flow pathway. Furthermore, the measured vertical core permeability is much less than that measured parallel to the bedding plane suggesting that CO_2 flow would be more likely parallel to the bedding plane than perpendicular to the bedding plane.

In addition, a similar study to probe the geochemical interactions of the CO_2/brine/rock system under geologic CO_2 storage conditions was conducted using core samples obtained from the Lower Tuscaloosa formation at the Plant Daniel CO_2 storage test site (Jackson County, Mississippi) [25]. The study reported a 7% decrease in porosity and a 13% decrease in permeability in the sandstone core after it was exposed to CO_2-saturated brine for six months. The decrease was due to feldspar dissolution, migration, and secondary mineral precipitation altering the sandstone pore/crack structure. The low content of active mineral phases in the Lower Tuscaloosa sandstone sample and the high initial porosity of the sample lead to a smaller permeability change for the sample after six months of exposure.

Therefore, the injection of CO_2 into a deep saline aquifer affects porosity since the dissolved CO_2 can cause mineral dissolution as well as precipitation in the formation. The change of porosity due to mineral reactions may adversely influence the permeability. This permeability change depends not only on the porosity, but also on the details of the pore space geometry and the distribution of precipitates within the pore space. During CO_2 storage in geologic formations, it is expected that supercritical CO_2 will dissolve into the formation's brine. The CO_2-charged brine becomes acidic and can react with minerals in the host deposit leading to dissolution, transport and reprecipitation which could affect the permeability.

The Lawson and Cedar Keys Formations of the South Florida Basin at a depth of between 900 and 4,000 m are potential CO_2 storage reservoirs in Florida. The rocks consist of porous dolostone sealed by the thick anhydrites of the overlying middle Cedar Keys Formation. The Lawson and Cedar Keys Formations have an average thickness of 200 m and average porosity of 20 percent. This deposit covers an area of about 91,000 sq. km (22,454,000 acres) [26]. Many of the porous beds within the Cedar Keys-Lawson storage reservoir exhibit lateral continuity and have average porosity around 20 percent. The estimated CO_2 storage capacity for the reservoir is approximately 97 billion tons of CO_2 which implies the Lawson and Cedar Keys Formations together could potentially support CO_2 sequestration for the large-scale power plants within this area for their entire 40-year lifespan [27]. The Cedar Keys-Lawson injection zone is a saline aquifer located below Tampa Electric at the Big Bend Power Station in Ruskin, Florida. The project was announced in 2010 and has since ended.

Although the project ended, there is still value in studying the CO_2/brine interaction effects on the Cedar Keys-Lawson formation to better our understanding of CO_2 sequestration in this type of geological formation. Core samples from the Cedar Keys-Lawson dolostone were placed in CO_2 saturated brine at sequestration temperature and pressure for a period of six, twelve and twenty-four months. These samples were studied *via* petrography, x-ray diffraction (XRD) and scanning electron microscopy-energy dispersive spectroscopy (SEM-EDS) to determine the mineralogical, textural, and geochemical changes that resulted from CO_2 exposure. Since the ability to predict how CO_2 will act in subsurface reservoirs relies on a detailed comprehension of the geochemical, mineralogical, and petrophysical

properties of reservoir and seal materials on microscopic to macroscopic scales, the understanding of geochemically induced changes in the porosity and permeability of the Cedar Keys-Lawson sandstone will strengthen our ability to predict CO_2 storage capacity and long-term reservoir behavior. Indeed, a recent review by Aminu and colleagues [2] suggested that rock minerals/brine/CO_2 interaction and its impact on storage reservoir quality (porosity and permeability) is a topic warranting further investigation.

MATERIALS AND METHODS

Core samples and brine

The Cedar Keys-Lawson injection zone is a saline aquifer positioned below Tampa Electric at the Big Bend Power Station in Ruskin, Florida. The formation is comprised of high porosity dolostone. The Cedar Keys-Lawson dolostone samples were collected from a depth of 1,207 m from a well located at Polk Power Station in Polk County, Florida. Three core samples approximately 2.54 cm in diameter x 5.08 cm in length were prepared. Two samples were cored perpendicular and one was cored parallel to the bedding plan (Table 1). The major mineral composition of the dolostone sample is 90% dolomite, with the balance including anhydrite, gypsum, celestine, quartz, and halite as determined by XRD. Synthetic brine samples were prepared as two-liter batches by mixing reagent grade salts of $CaCl_2{\cdot}2H_2O$ (73.364 g), $FeSO_4{\cdot}6H_2O$ (0.956 g), KCl (0.763 g), $NaHCO_3$ (0.551 g), Na_2CO_3 (0.403 g), NaBr (1.03 g), NaCl (202.92 g), Na_2SO_4 (0.083 g), NH_4Cl (0.593 g), $MgCl_2{\cdot}6H_2O$ (16.729 g), and $SrCl_2{\cdot}$ 6 H_2O (3.04 g) in nitrogen-purged deionized water under constant stirring. Solutions were filtered through 0.45 μm paper filter to remove any particulates prior to use. Mean concentrations from the analysis of dissolved constituents in brine filtrate are listed in Table 2.

Table 1. The change of permeability and porosity of the core interacted with CO_2/brine for six, twelve and twenty-four months under CO_2 sequestration conditions.

	Unreacted	**Reacted**	**Unreacted**	**Reacted**	**Unreacted**	**Reacted**
Duration (month)	Fresh	6	Fresh	12	Fresh	24
Cored direction	Parallel	Parallel	perpendicular	perpendicular	perpendicular	perpendicular
Obtained depth (m)	1,207		1,207		1,207	
Size (cm)	2.54 (O.D.) x 5.08		2.54 (O.D.) x 5.08		2.54 (O.D.) x 5.08	
Major ~ 90%	Dolomite		Dolomite		Dolomite	
Minor < 10%	Anhydrite, gypsum, celestine, quartz, and halite		Anhydrite, gypsum, celestine, quartz, and halite		Anhydrite, gypsum, celestine, quartz, and halite	
Porosity, %	24.4	24.1	28.0	27.6	28.8	27
Permeability (mD)	44	47	3.1	3.3	2.13	1.63
pH	6.02	5.75	6.05	5.58	6.02	5.49

Table 2. The analysis of fresh synthetic brine and the brine after interaction with CO_2/core minerals for periods of six, twelve and twenty-four months under CO_2 sequestration conditions.

	Fresh brine batch #3	**Reacted brine after 6 months**	**Fresh brine batch #4**	**Reacted brine after 12 months**	**Fresh brine batch #3**	**Reacted brine after 24 months**
	ppm	**ppm**	**ppm**	**ppm**	**ppm**	**ppm**
Ca	9833	11115	11509	12035	9833	9907
Fe	46	~	670	209	46	31
K	809	981	354	413	809	811
Mg	788	1148	890	1132	788	927
Na	38290	43332	35454	35773	38290	34097
S	40	77	49.1	75.9	40	125
Si	~	10	~	9.49	~	10.5
Sr	454	265	466	377	454	214
Cl	72662	72478	87421	83433	72662	66962
Br	214	214	389	389	214	214
$SO_4^{=}$	220	455	163	805	220	331
pH	6.02	5.75	6.05	5.58	6.02	5.49

Reactors and experimental procedures

Three 1.8 liter (N4683-T-HC-7500 C276) high-pressure vessels (9.53 cm I.D. x 26.67 cm depth) manufactured by Parr Instrument Company, Erie, Pennsylvania, were used for this study. An open Teflon cell (7.62 cm I.D. x 10.16 cm length) and a smaller Teflon reaction cell insert (6.35 cm I.D. x 9.52 cm length) were utilized inside the pressure vessels. An ISCO 260D syringe pump was used to charge each vessel with CO_2 and to maintain the pressure in the reactor. Temperatures were maintained within ±1 °C. A diagram of the reaction system is shown in Figure 1.

In a typical experiment, after loading a smaller Teflon container holding the samples (core and two small chip samples with a volume ratio of brine to core of 5) and brine into a larger Teflon container, the larger container was placed into the pressure vessel. The gap between the two Teflon containers was then filled with brine to ensure that the CO_2 phase was saturated with water vapor without substantially altering the salt concentration in contact with the core sample. The pressure vessel was then purged with CO_2 three times to remove residual air.

Finally, the vessel was charged with approximately 4.08 MPa (592 psig) of CO_2 and then slowly heated to a final temperature of 55 °C. During the heating period of about four hours, CO_2 was slowly added to the vessel until the desired testing pressure of 23.8 MPa (3,500 psig) was reached. The three vessels were maintained at these conditions for six months (first vessel), twelve months (second vessel) and twenty-four months (third vessel). Upon completion of the experiment, the temperature of the reactor was reduced to ambient temperature, then the CO_2 was slowly vented and the sample was removed. The solid samples were rinsed with deionized water multiple times to remove residual brine and then dried in a desiccator under flowing N_2. Liquid from the sample-bearing container was recovered

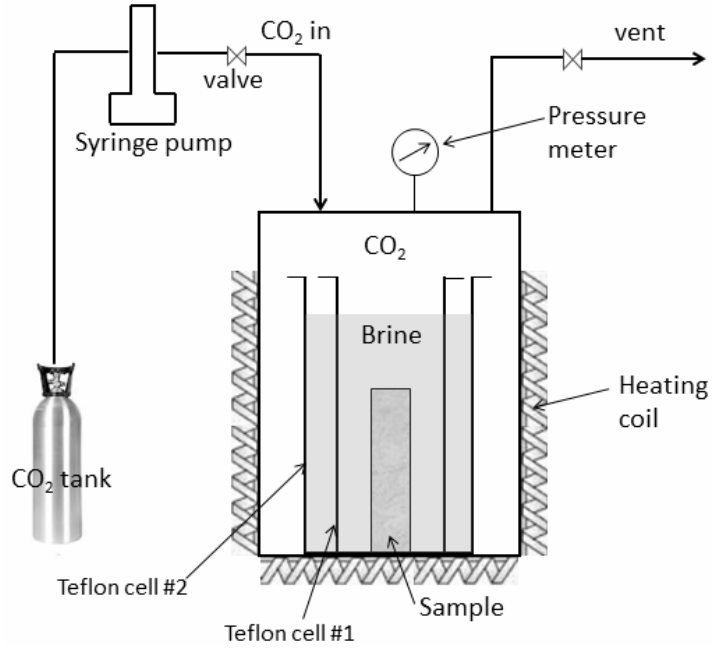

Figure 1. Static reactor system for CO_2-brine-rock study.

for analysis. The compositional analysis results of the reacted brine are reported in Table 2.

Analytical methods

Measurements and analysis methods

Before and after the CO_2/brine exposure tests, the solids were characterized by computed tomography (CT) scanning, x-ray diffraction (XRD), and scanning electron microscopy (SEM)-energy dispersive x-ray spectroscopy (EDS). Inductively coupled plasma-optical emission spectroscopy (ICP-OES) was utilized to determine metal concentrations in the liquid samples, but due to high salt concentrations, sample dilution with distilled/deionized water was required. Solutions were analyzed for the full range of metals quantifiable by ICP-OES including Al, Si, and Fe. The details of cation and anion analyses, XRD, and SEM-EDS analyses have been reported elsewhere [28].

Porosity and permeability of the samples were measured both before and after exposure. The porosity was measured using a helium porosimeter (HP-401, TEMCO, Inc., Tulsa, OK) at 0.7 MPa at ambient temperature. For three core samples, a TEMCO Ultraperm 500 "flow-through" permeameter was used to measure the permeabilities [20]. The permeability of the core samples was measured at a confining pressure of 11.63 MPa approximating the depth at which the core was collected. Various effective pressures were utilized to obtain the permeability profile of the core. The porosity and permeability measurements are illustrated in Table 1.

All of the cores were scanned in a Zeiss Versa-X 400 micron CT scanner. Each of the reconstructed pre- and post-images of the 2.54 cm diameter dolomite cores have a voxel resolution between 15.7 and 15.5 μm with 1,440 images. All resolutions used were not fine enough to resolve the micro- to nano-scale porosity present in the dolomite. The undetectable pores may connect larger voids that facilitate mass transport. Instrument settings, operating conditions, and scan parameters are described elsewhere [25]. The reconstruction properties of the images were selected to provide the highest fidelity rendition of the scanned sample and to construct a 3-D volumetric representation of the core. The data were exported as a series of 16-bit grayscale cross-sectional TIFF images. Image post processing was performed using the open-source software ImageJ and was reported elsewhere [25].

RESULTS AND DISCUSSION

To investigate the interaction between the cores from the Cedar Keys-Lawson formation and CO_2/brine under CO_2 storage conditions, the following experiments were conducted. The cores were exposed to CO_2/brine at 55 °C and 23.8 MPa of CO_2 for six, twelve and twenty-four months in the static reactors. The porosity measurements conducted on the three core samples showed a similar trend (Table 1); the host reservoir rock exhibits a decrease in porosity by 1.2, 1.4, and 6.25% with respect to six, twelve, and twenty-four-month CO_2/brine exposure. The measured permeability shows a different trend. The permeability for six- and twelve-month exposure experiments shows an increase of 6.8 and 6.4% respectively. However, a 23% decrease of permeability after the twenty-four month experiment was observed.

Six- and twelve-month results

The observations obtained from the six- and twelve- month exposure experiments are similar thus they are discussed together. The porosity quantification obtained from the sample showed a slight decrease from 24.4% to 24.1% for the core after it was exposed to CO_2-saturated brine for six months (Table 1). Furthermore, the porosity measurements showed a decrease from 28.0% to 27.6% (Table 1) for the twelve month exposure experiment. The decrease of porosity might suggest the precipitation of minerals within the core. The change in permeability showed a different trend (Table 1), the post six month exposure permeability of 47 mD from the core was about 6.8% higher than the measured pre-reaction permeability of 44 mD in the fresh core. The post twelve month exposure permeability of 3.3 mD was increased slightly from 3.1 mD of the fresh core. This result implies that the CO_2/brine exposure may change the pore characteristics by enhancing flow and resulting in permeability increases.

Figure 2 shows CT analysis results of the core before and after the six-month exposure environment. The pre- (A) and post- (B) six-month exposed samples were CT scanned in top and bottom sections and stitched together for analysis. Pre-exposure scans (A) were completed at 15.4 μm resolution and post-exposure (B) were scanned at 15.1 μm resolution each with 1,440 radiographs in the YZ-plane. The pre- and post-exposure scans are similar in location for each image pair. Both pore space (dark zones) and higher attenuating minerals within the core (bright zones) can be observed. The high attenuating material located in the pore space highlighted by the boxed areas (Figure 2B) was not present in the pre-exposure scan (Figure 2A). This provides evidence of mineral precipitation after the core was exposed to the CO_2-brine environment. The high attenuating material located in the pore space highlighted by the circled areas (Figure 2A) was less dense in the post-exposure scan (Figure 2B). This implies dissolution took place during exposure. Furthermore, larger dark zone in the circled area was observed in the post-exposure (Figure 2B) *vs*. pre-exposure (Figure 2A). This suggests void was created after the six-month exposure. The mineral dissolution can also be observed by comparing the higher attenuating material within the same circled area (Figure 2A (pre-exposure)) *vs*. that in Figure 2B (post-exposure).

Figure 3 highlights a region of interest in the XY-plane where the pore space adjacent to the core edge increased during CO_2-saturated brine exposure. Comparing the boxed area between pre- (Figure 3A) and post- exposure (Figure 3B) showed more attenuating minerals in the post-exposure (Figure 3B) or precipitation. Both pore space (dark zones) and higher attenuating minerals within the core (bright zones) can be observed in Figure 3A and 3B. It can be seen in the boxed areas that a highly attenuating mineral appeared, Figure 3B, after the six-month exposure to CO_2-saturated brine. The new mineral precipitation may reduce the measured porosity after six months. In contrast, in the lower right corner of the image in the circled areas, mineral dissolution was observed after the sample was exposed to CO_2-saturated brine for six months. In addition, a larger/connected dark zone in the circled area was observed in the post-exposure (Figure 3B) vs. pre-exposure (Figure 3A). The net effect of mineral dissolution and mineral precipitation occurring in the sample pores and cracks resulted in the observed 6.8% increase in permeability. This implies more void space was

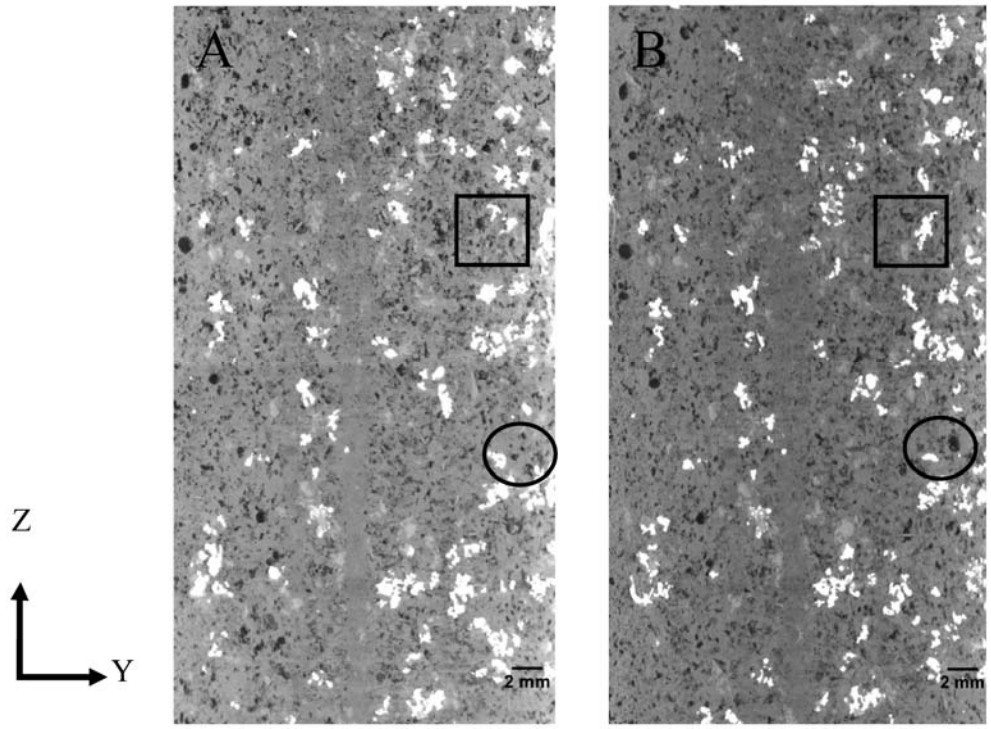

Figure 2. (A) Pre and (B) Post-exposure in the YZ-plane.

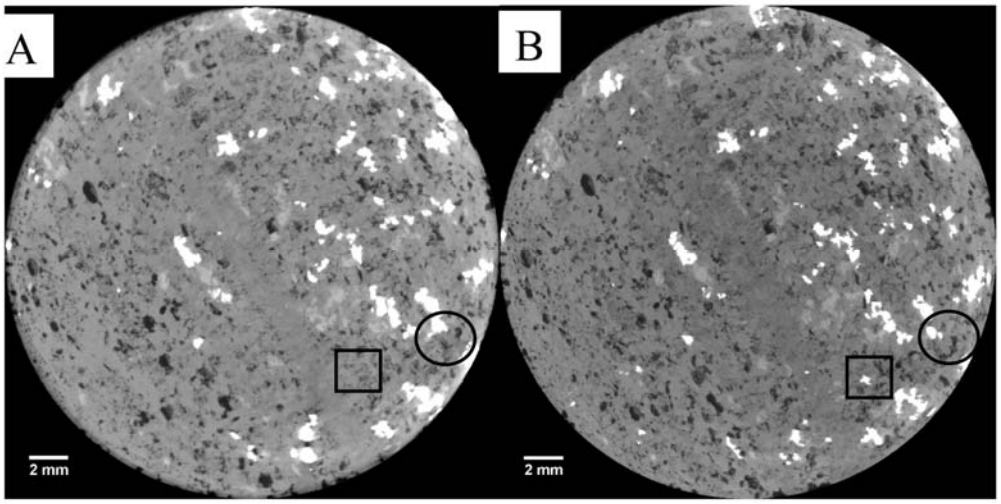

Figure 3. (A) Pre and (B) Post-exposure slice in the XY-plane.

created/connected after the six-month exposure. The large void present in the post exposure slice (Figure 4B) highlighted by the boxed area was not present prior to exposure (Figure 4A). Smaller pores also formed within this region of interest. The newly formed pore space observed in Figure 4B clearly indicates the degree of dissolution that occurred during exposure. It is noted that the dissolution that occurred during the six-month exposure enhanced the connectivity between voids. This may contribute to the increase of permeability after the CO_2/brine exposure.

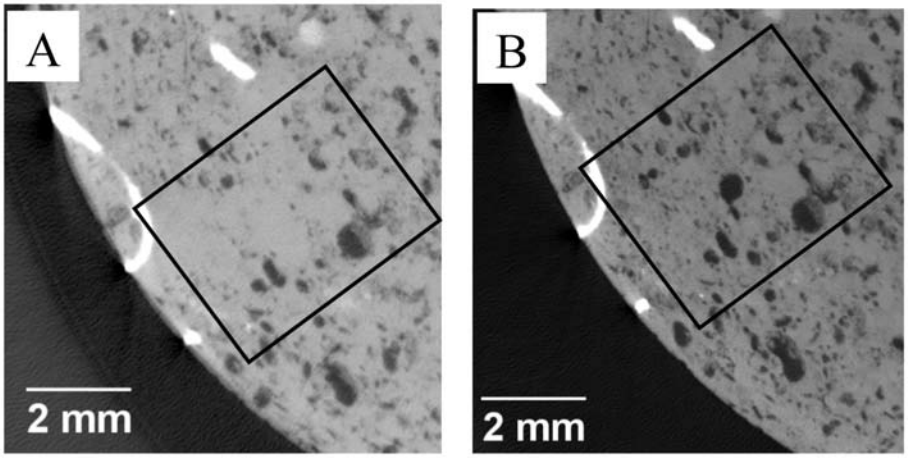

Figure 4. Top: (A) Pre- and (B) Post-exposure region of interest in the XY-plane.

Figure 5A (fresh) and 5B (exposed) show backscattered SEM images of the core sample. In the circled area of the before and after images, evidence of partial gypsum/anhydrite dissolution is observed after the six-month exposure to CO_2/brine. SEM shows etching on the surface of gypsum/anhydrite in the upper left area (Figure 5B) after exposure to the sequestration conditions. This mineral dissolution could result in more flow pathway connections contributing to the observed increase in the measured permeability after six months. This observation is in accord with the finding from CT images (Figure 4). Figure 6A (fresh) and 6B (exposed) show the backscattered SEM images of the core sample in another area. The circled area in Figure 6B shows that the gypsum/anhydrite, identified based on EDS and XRD, has been partially dissolved by exposure to sequestration conditions. The boxed area in Figure 6A shows a celestine surface while the same area in Figure 6B clearly shows the celestine has grown in size with well-formed crystal faces. EDS indicates celestine regrew on fractured, preexisting celestine surfaces. These same results were observed in multiple areas of the sample. The post-exposure Sr concentration also shows a decrease (Table 2). The decrease in Sr concentration may be due to the growth/precipitation of celestine.

SEM images (Figure 7A, B) were taken after the samples were exposed to the brine and CO_2 for twelve months. Celestine shows recrystallization (Figure 7B) in the boxed area as well as in the large region to the left of the boxed area after twelve-month exposure. This is probably due, at least in part, to the presence of Sr in the brine since the concentration of Sr in the reacted brine decreased (Table 2). The void in the circled area (Figure 7A and 7B) shows evidence of increasing in size after twelve-month exposure. This change could be due to dissolution of dolomite. The SEM images showed the same trends in mineral precipitation/dissolution as were observed after six months of exposure. Another site (Figure 8B) in the boxed area showed the deposition of a secondary Fe phase on the dolomite, possibly a hydrated Fe oxide, hematite, or siderite. This observation of high Fe concentration was also observed for similar morphology particles at other sample sites. The dolomite in the circled area (Figure 8B) shows evidence of dissolution after twelve-month exposure.

The post-reaction brine was analyzed following contact with the core samples and CO_2 (Table 2). Comparing the reacted brine with the fresh brine, the following trends were observed. The concentrations of Ca, K, Mg, Na, S, Si, and $SO_4^{=}$ increased. The concentrations of Fe and Sr decreased after the six- and twelve-month exposure period. The combined information suggests both the dissolution of dolomite and gypsum contribute to the observed changes. The pH was reduced from 6.02 to 5.75 after the six-month exposure experiment and from 6.05 to 5.58 after the twelve-month exposure experiment.

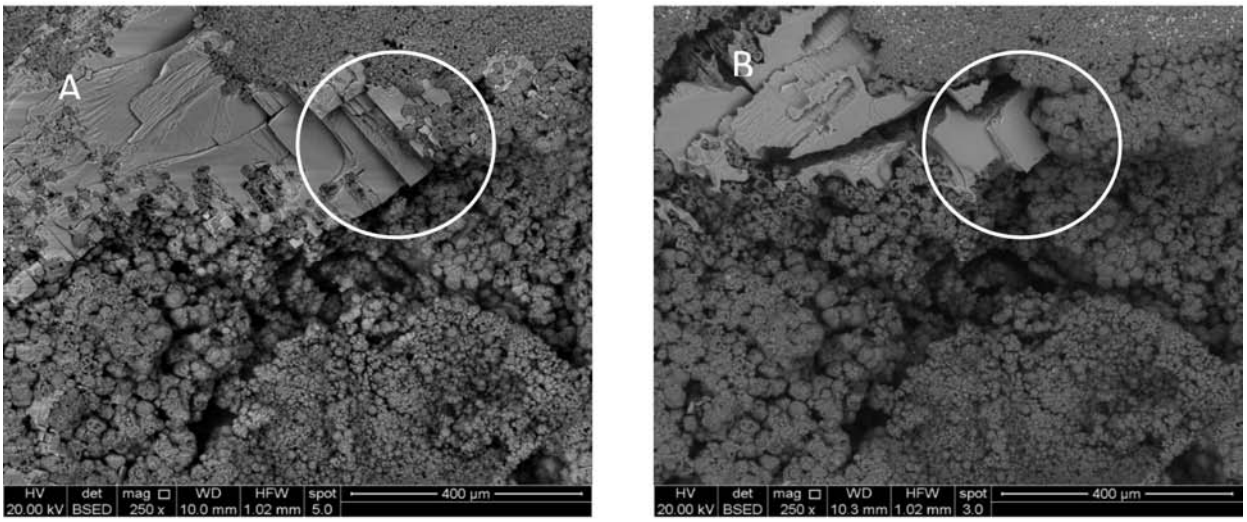

Figure 5. A (fresh) and B (exposed). SEM images of sample before and after exposure to CO_2/brine under CO_2 sequestration conditions for six months.

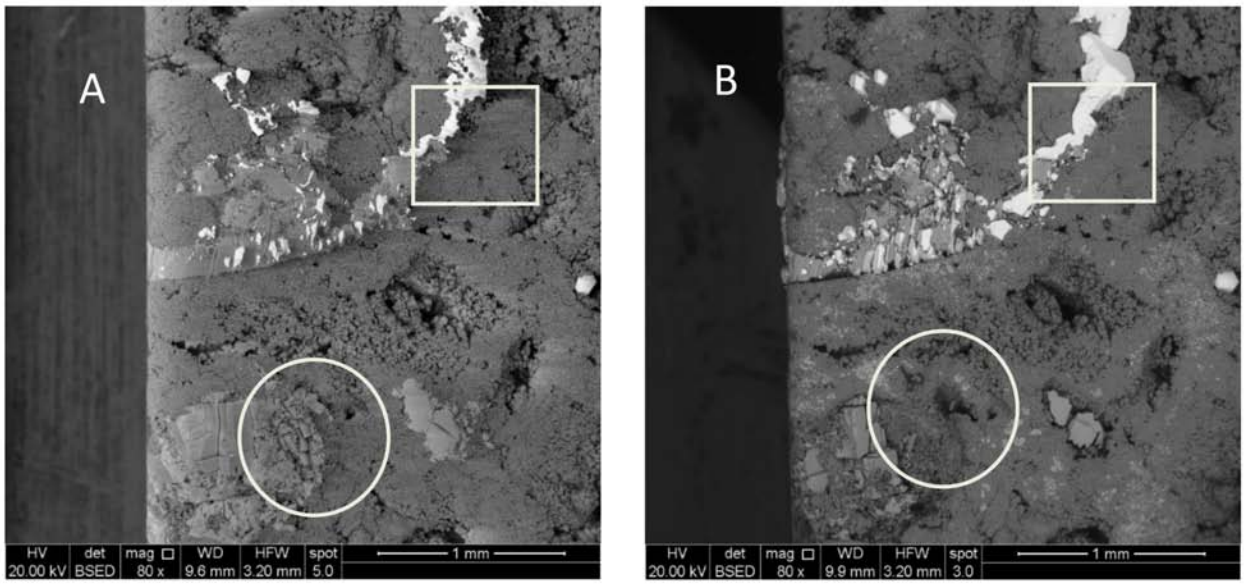

Figure 6. SEM images of fresh sample (A) *vs.* sample exposed to CO_2/brine for six months (B).

Solution chemistry suggested that CO_2-acidified brine may preferentially dissolve gypsum ($CaSO_4{\cdot}2(H_2O)$) and dolomite ($CaMg(CO_3)_2$) which correlates with the increase in the concentration of sulfate, Ca, and Mg in the reacted brine (Table 2). The concentration of Fe decreased after the six- and twelve-month exposure period. This decrease is likely due to the precipitation of Fe minerals as observed by SEM/EDS. The following observations were noted by comparing the solution chemistry before and after exposure to CO_2. Szecsody *et al.* [19] studied the influence of supercritical CO_2 injection on precipitation, metal migration and changes in the Mount Simon sandstone cores obtained from Jacksonville, Illinois (38 °C and up to 12.4 MPa of CO_2 with the presence of brine in the flow through 1-D column). They reported

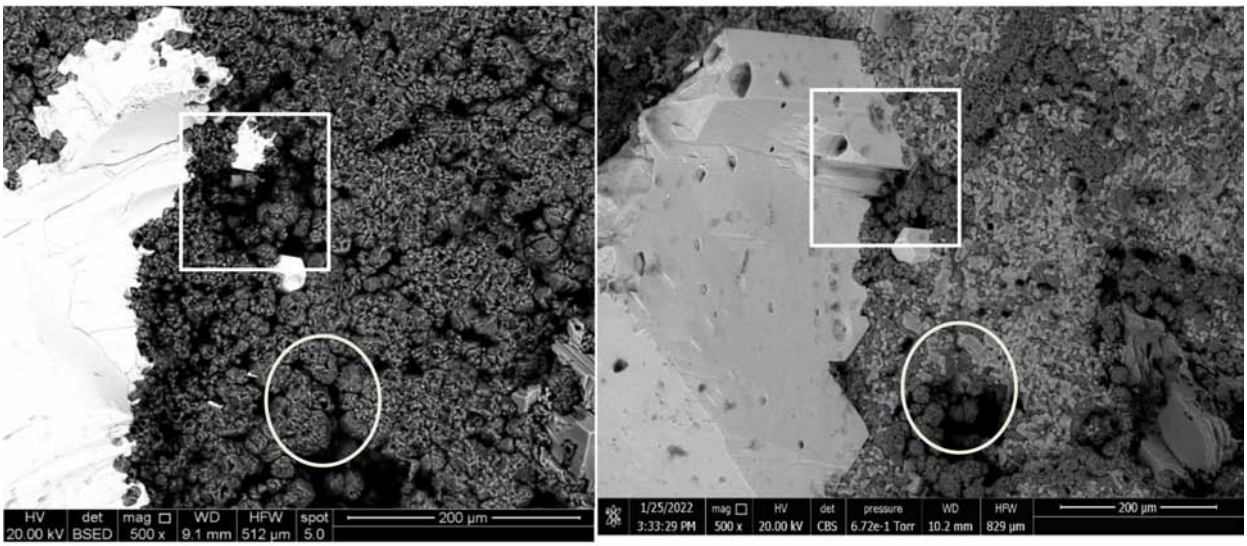

Figure 7. (A) Pre- and (B) Post-exposure. SEM images of sample before and after exposure to CO_2/brine under CO_2 sequestration conditions for twelve months.

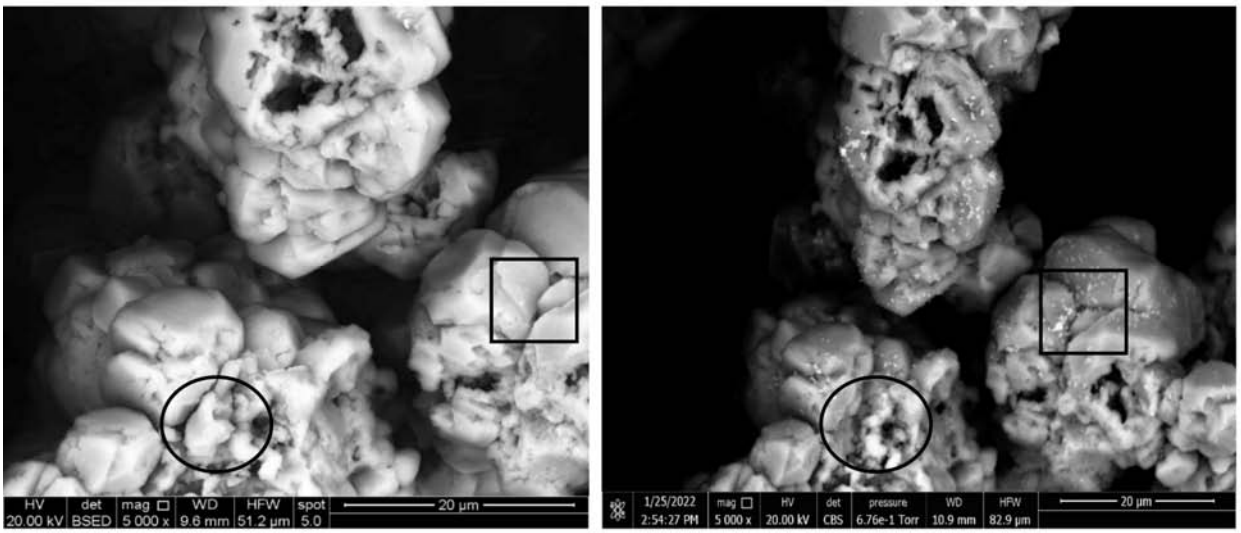

Figure 8. (A) Pre- and (B) Post-exposure. SEM images of sample before and after exposure to CO_2/brine under CO_2 sequestration conditions for twelve months.

short-term mineral dissolution, ion desorption and iron oxide particulate movement because of CO_2 displacement of the brine in larger pores. It has been reported that the permeability of the reservoir rock is affected by the combination of dissolution and precipitation of minerals [20]. Gouze and Luquot [5] have shown that the increase of permeability is due to the decrease of the tortuosity for homogeneous dissolution, whereas it is due to the combination of tortuosity decrease and hydraulic radius increase for heterogeneous dissolution. Norgues *et al*. [23] also reported that even dissolving the small amounts of cementing materials such as calcite, can change the permeability significantly.

Twenty-four month results

The porosity measurements conducted on the core sample showed a decrease from 28.8% to 27.0% (Table 1) after exposure to CO_2-saturated brine for twenty-four months. The decrease of porosity might suggest the precipitation of minerals within the core. Furthermore, the change in porosity also resulted in a change of permeability (Table 1). The permeability decreased from 2.13 to 1.63 mD following exposure. Core permeability decreased substantially by 23% during the experiment although core porosity only changed by 6.25%. The permeability reduction is probably the result of precipitation of new mineral phases such as those observed in Figures 9, 10, 11, and 12.

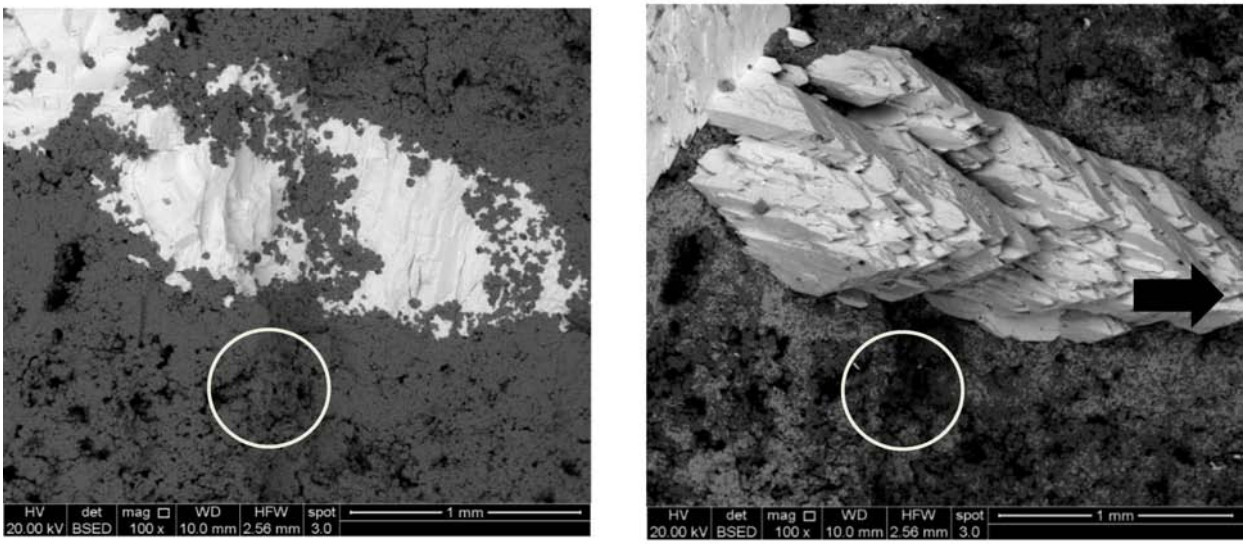

Figure 9. A (fresh) and B (exposed). The SEM images of sample after exposed to CO_2/brine under CO_2 sequestration conditions for twelve-four months.

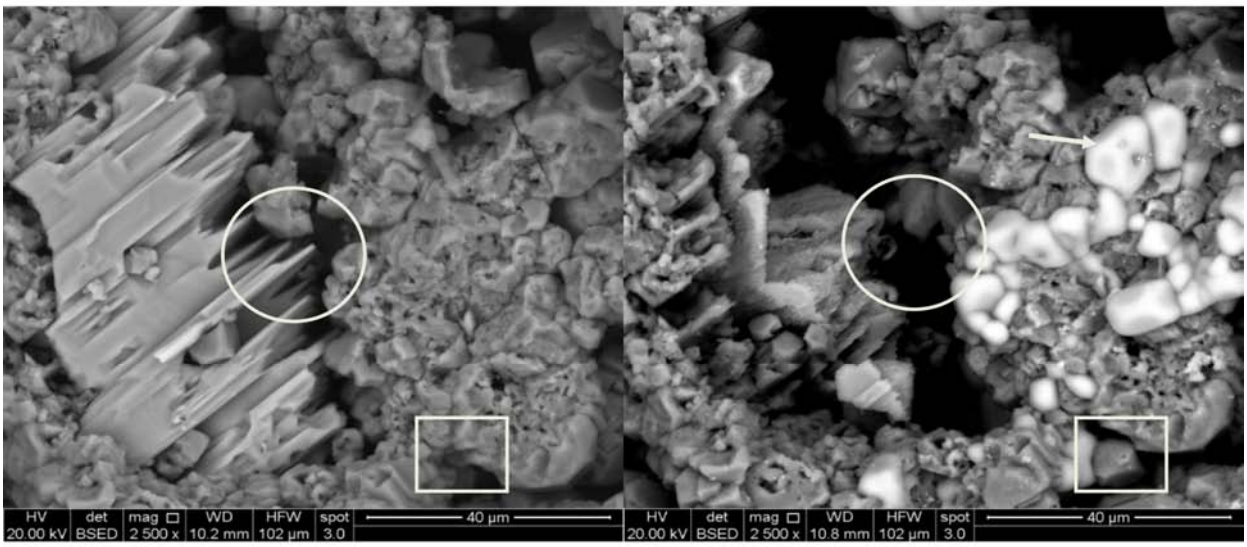

Figure 10. SEM images of fresh sample (A) *vs.* sample exposed to CO_2/brine for twelve-four months (B).

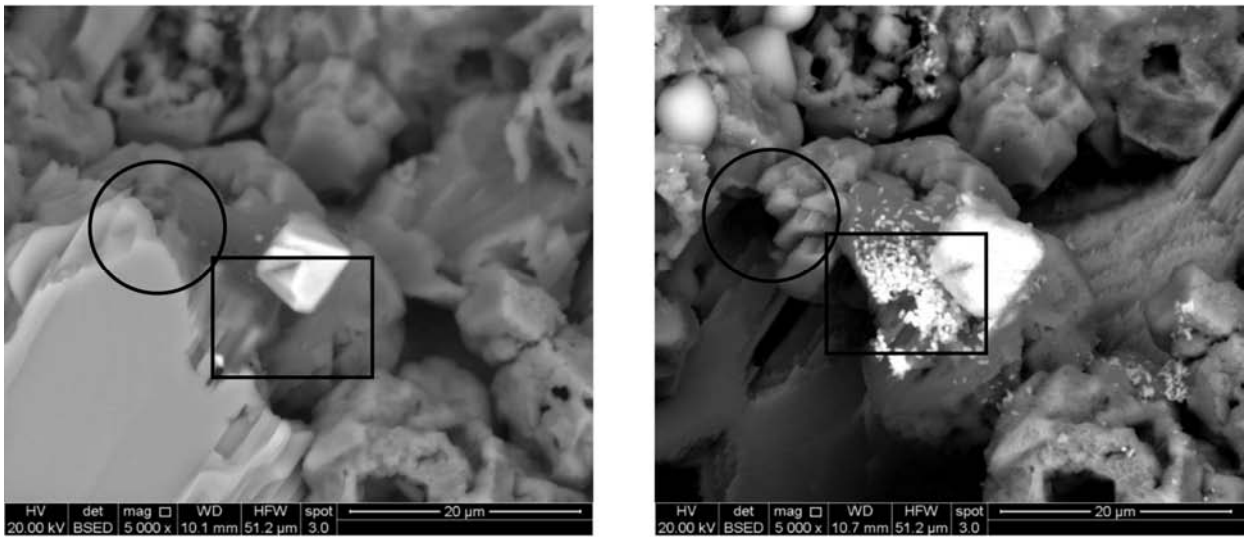

Figure 11. SEM images of fresh sample (A) *vs.* sample exposed to CO_2/brine for twelve-four months (B).

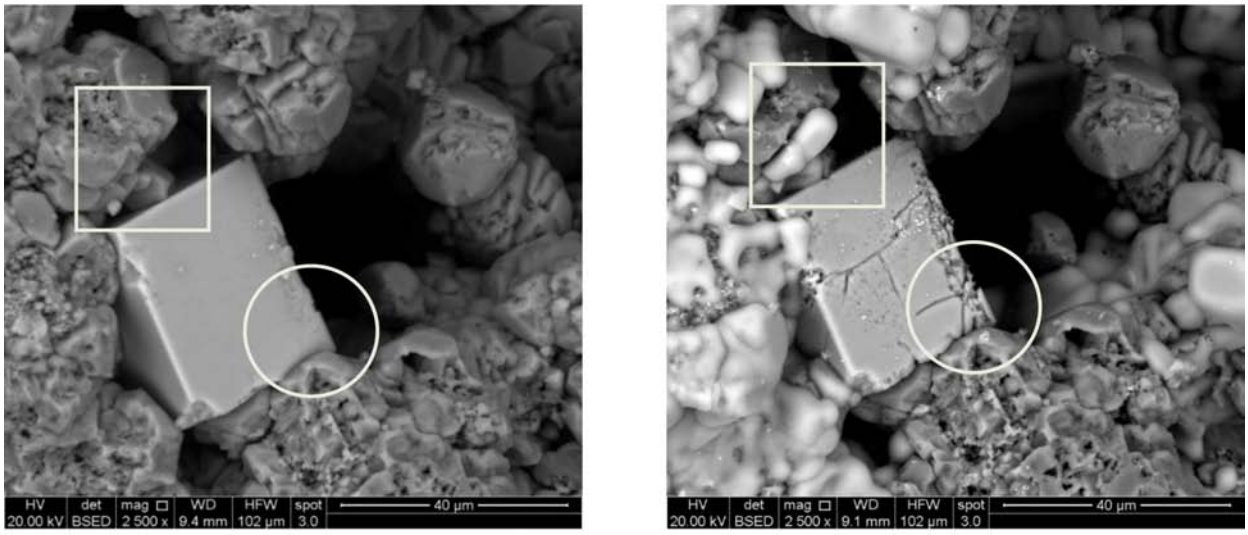

Figure 12. SEM images of fresh sample (A) *vs.* sample exposed to CO_2/brine for twelve-four months (B).

SEM images (Figure 9A, B) were taken after the samples were exposed to the brine and CO_2 for twenty-four months. The dolomite in the circled area (Figure 9B) shows evidence of dissolution after twenty-four month exposure. Significant celestine precipitation or recrystallization can be observed in Figure 9B (arrow). The gypsum/ anhydrite in the circled area (Figure 10B) shows evidence of dissolution after twenty-four month exposure. Some mineral precipitation is observed in the boxed area in Figure 10B. In addition, NaCl residue was evident (arrow). Another site (Figure 11B) showed the deposition of an Fe mineral (boxed area) adjacent to and on a pyrite crystal. The Fe mineral adjacent to and covering the pyrite crystal could be evidence of the alteration of pyrite during the exposure period. The gypsum/ anhydrite in the circled area (Figure 11B) shows evidence of dissolution after twenty-four month exposure. The boxed area in Figure 12B

highlights NaCl residue on the surface after the two-year exposure. The NaCl surface deposits observed were probably due to slow diffusion of residual brine out of pore structure to the surface. Furthermore, a fluorite crystal (CaF_2) in the circled area showed slight etching after the exposure. The XRD patterns for the dolomite sample reacted with CO_2 and brine *vs.* the fresh sample are compared in Figure 13. The XRD analysis of the Cedar Keys-Lawson sandstone showed some detectable differences in mineral composition following two years of exposure of CO_2 with brine. Celestine and halite intensities increased, and gypsum intensity decreased. Celestine precipitation can be easily seen in Figure 9. The reduced concentration of Sr can also be observed (Table 2). The reacted sample contained significant NaCl likely due to the difficulty in washing the residual brine from the porous matrix of the core samples. The NaCl surface deposit was probably formed due to slow diffusion of residual brine out of pore structure to the surface during drying, which is commonly referred to as a "salting out" effect. The combined salting out effect, celestine precipitation along with Fe deposit (Figure 11) as well as mineral precipitation observed (Figure 9) resulted in the decrease in porosity and permeability after the two-year exposure experiment. The decreasing concentration of Fe may be related to the precipitation of hematite (Fe_2O_3) or another Fe mineral such as siderite ($FeCO_3$) (Figure 11B). The precipitation of siderite could be due to the interaction between Fe in the solution with dissolved CO_2 in the brine under current experimental conditions. The combination of dolomite, anhydrite, and gypsum dissolution as well as the precipitation of secondary minerals and NaCl contribute to a decrease in bulk permeability.

The post-reaction brine was analyzed following contact with the core and CO_2 (Table 2). Comparing the reacted brine with the fresh brine, the following trends were observed. The concentrations of Fe, Na, Cl and Sr were decreased. The concentrations of K, Ca, Mg, S, and $SO_4^{=}$ increased after the two-year exposure

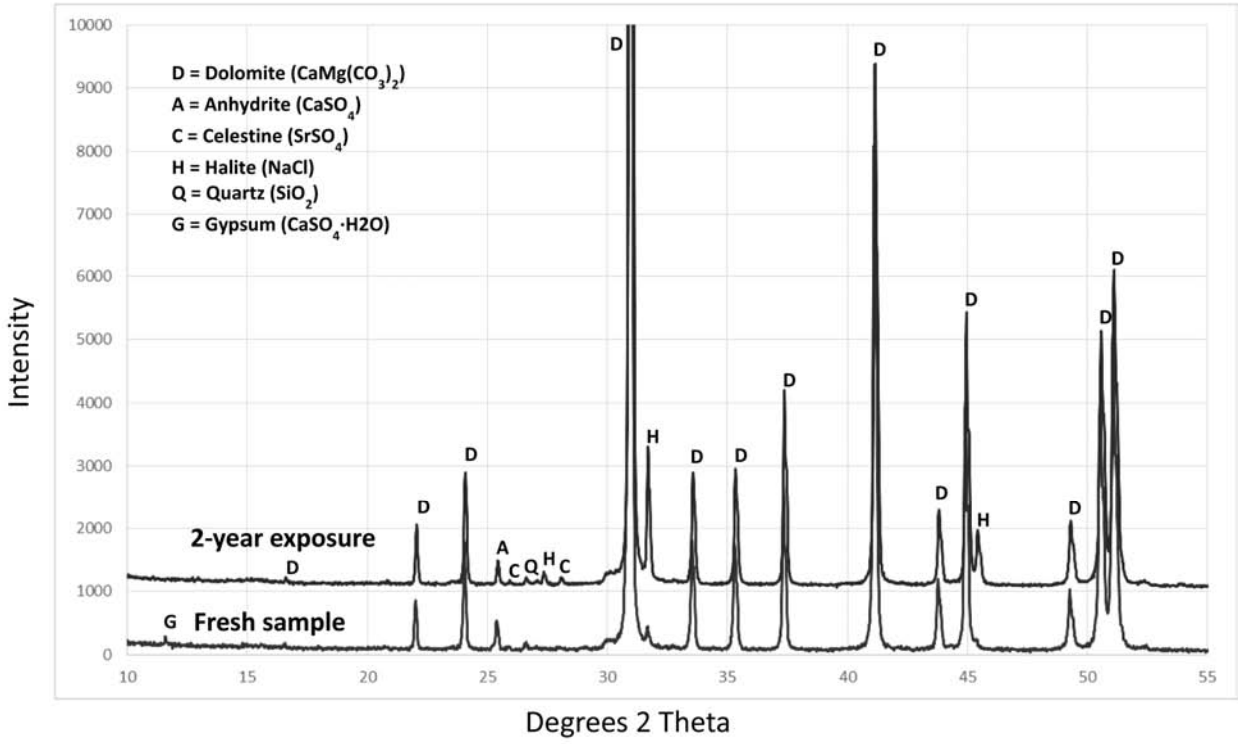

Figure 13. XRD scans of the fresh sample vs. 2-year exposed sample.

period. The pH was reduced from 6.02 to 5.49 after the two-year exposure experiment. The sample is composed mainly of dolomite, which has a lower dissolution rate and less reactivity than anhydrite and gypsum. Solution chemistry indicated that CO_2-acidified brine has dissolved some dolomite, anhydrite, gypsum, as well as possibly quartz and resulted in the observed increases in concentrations. Thus, an increase in the concentration of sulfate, Ca, and Mg in the reacted brine were noted for up to twenty-four-month exposure experiments (Table 2). The decrease in concentration of Sr is related to the observed celestine growth or precipitation. The decreasing concentration of Fe may be related to the precipitation of hematite (Fe_2O_3) or another Fe mineral such as siderite ($FeCO_3$) or a hydrated Fe oxide. The concentration was too low for confirmation by XRD. As stated above, the precipitation of siderite could be due to the interaction between Fe in the solution with dissolved CO_2 in the brine under the experimental conditions.

With the experimental results obtained and analyzed so far, the host reservoir rock already exhibits a decrease in porosity by 1.2, 1.4, and 6.25% with respect to six, twelve- and twenty-four-month CO_2/brine exposure experiments. The decrease of porosity is related to mineral precipitation and NaCl precipitation. The NaCl precipitation is more significant after the twenty-four month exposure experiment as can be observed in Table 2, XRD results and SEM images (Figure 10B and Figure 12B). The measured permeability shows a different trend. The permeability for six- and twelve-month exposure experiments shows an increase of 6.8 and 6.4%, respectively. The increase may relate to the increase of pore void as can be seen from Figure 4B (six-month exposed sample). The enhancement in pore void/connectivity thus increases the measured permeability. The 23% decrease of permeability after the twenty-four month experiment may be due to NaCl as well as mineral precipitation resulting in the loss of connectivity between pores. A similar result has been described by Gui *et al*. [29] suggesting that salt precipitation is a coupled process of gas-liquid seepage and mineral crystallization. Under the effect of mass transfer between CO_2 and water phases, the water molecules constantly evaporate and diffuse into CO_2, resulting in the precipitation of dissolved salt in the formation water. The precipitated salt would migrate under the drag force of the injected CO_2 ad then accumulate in pore throats, reducing the reservoir permeability.

It is also noted that the measured permeability of a fresh core orientated perpendicular to the bedding plane (around 3.1 and 2.13 mD) is one order of magnitude less of that from a core orientated parallel to the bedding plane (around 44 mD) (Table 1). This suggests CO_2 flow would be more likely parallel to the bedding plane than perpendicular to the bedding plane.

Combined data from SEM-EDS, XRD, CT scanning, and brine analysis indicate dissolution of minerals, most likely anhydrite/gypsum and dolomite in flow pathways along with precipitation of Fe-related minerals, celestine, and halite on the external surfaces as well as in flow pathways. The net effect was an increase of permeability for up to twelve months of CO_2/brine exposure. However, for the longer CO_2/brine exposure, precipitation of Fe minerals, celestine, and halite had the net effect of decreasing permeability.

CONCLUSION

An experimental study of the interaction of CO_2/brine/rock modelling saline formations was conducted in a static system under CO_2 storage conditions. Core samples consisting of primarily porous dolostone from the Cedar Keys-Lawson Formation in Florida were investigated. Chemical interactions of the core carbonate upon exposure to CO_2 and brine under sequestration conditions were studied. Samples were exposed to simulated *in-situ* reaction conditions for six-month, twelve-month, and twenty-four-month periods.

In a typical experiment, a core sample with a model brine was reacted under static conditions at 55 °C and a CO_2 pressure of 23.8 MPa (3,500 psig). CT, XRD, SEM-EDS, brine chemistry, porosity, and permeability analyses were conducted prior to and after the experiments.

The host reservoir rock exhibits a decrease in porosity of 1.2, 1.4, and 6.25% with respect to

six, twelve- and twenty-four-month CO_2/brine exposure experiments. The decrease of porosity is related to mineral precipitation and NaCl precipitation. The NaCl precipitation is more significant after twenty-four month exposure. The permeability for six- and twelve-month exposure experiments shows an increase of 6.8 and 6.4 %, respectively. The increase may relate to the increase of pore connectivity thus increasing the permeability. This observation suggests that mineral dissolution and mineral precipitation could occur in the host deposit altering its characteristics for CO_2 storage over time. Both SEM and CT images of the exterior surface as well as pore space clearly illustrate the degree of dissolution that occurred during exposure. Mineral dissolution (dolomite, anhydrite, and gypsum) was observed during the exposure and was found to be more significant after the six-month exposure, likely enhancing the connectivity between the voids. This probably contributed to the change of permeability after the CO_2/brine exposure. The 23% decrease of permeability after the twenty-four month experiment likely relates to NaCl and mineral precipitation blocking the connectivity of pores.

It is also noted that the measured permeability of fresh core orientated perpendicular to the bedding plane is one order of magnitude less of that from a core orientated parallel to the bedding plane. This suggests CO_2 flow would be more likely parallel to the bedding plane than perpendicular to the bedding plane.

ACKNOWLEDGEMENTS

We thank Bryan Tennant for providing the CT images of the studied rock samples. We are also indebted to Dr. R. H. Lin for the preparation of the brine and to Leidos Research Support Team for conducting the brine samples analysis.

CONFLICT OF INTEREST STATEMENT

There are no conflicts of interest.

DISCLAIMER

This report was prepared as an account of work sponsored by an agency of the United States Government. Neither the United States Government nor any agency thereof, nor any of their employees, makes any warranty, express or implied, or assumes any legal liability or responsibility for the accuracy, completeness, or usefulness of any information, apparatus, product, or process disclosed, or represents that its use would not infringe privately owned rights. Reference herein to any specific commercial product, process, or service by trade name, trademark, manufacturer, or otherwise does not necessarily constitute or imply its endorsement, recommendation, or favoring by the United States Government or any agency thereof. The views and opinions of authors expressed herein do not necessarily state or reflect those of the United States Government or any agency thereof.

REFERENCES

1. MacDowell, N., Florin. N., Buchard, A., Hallett. J., Galindo. A., Jackson. G., Adjiman. C., Williams, C., Shah, N. and Fennel, P. 2010, Energy & Environmental Sci., 3, 1645.
2. Aminu, M. D., Nabavi, S. A., Rochelle, C. A. and Manovic, V. 2017, Applied Energy, 208, 1389.
3. Ali, M., Jha, N. K., Pal, N., Kesharz, A., Hoteit, H. and Sarmadivaleh, M. 2022, Earth-Science Reviews, 225, 103895.
4. Dziejarski, B., Krzyznska, R. and Andersson, K. 2023, Fuel, 342, 127776.
5. Luquot, L. and Gouze, P. 2009, Chemical Geology, 265, 148.
6. Morse, J. W. and Arvidson, R. S. 2002, Earth Science Reviews, 58, 51.
7. Jove-Colon, J. F. Oelkers, E. H. and Schott, J. 2004, Geochimica et Cosomochimica Acta, 68, 805.
8. Liu, F., Lu, P. Zhu, C. and Xiao, Y. 2011, Inter. J. Greenhouse Gas Control., 5, 294.
9. Shi Z, Sun L, Haljasmaa I., Harbert, W., Sanguinito, S., Tkach, M., Goodman, A., Tsotsis, T. and Jessen, K. 2019, J. Petroleum Science and Engineering, 77, 295.
10. Amonette, J., Johnson, T., Spencer, C., Zhong, C., Szecsody, J. and Vermeul, V. 2014, Energy Procedia, 63, 4095.

11. Bonneville, A., Gilmore, T., Sullivan, C., Vermeul, V., Kelley, M., White, S., Appriou, D., Bjornstad, B., Gerst, J., Gupta, M., Horner, J., McNeil, C., Moody, M., Pike, W., Spane, F., Thorne, P., Zeller, E., Zhang, E., Hoffmann, J. and Humphreys, K. 2013, Energy Procedia, 37, 6125.
12. Zhang, L. Soong, Y. Dilmore, R. M. and Lopano, C. 2015, Chemical Geology, 403, 1.
13. Soong, Y., Howard, B. H., Dilmore, R. M., Haljasmaa, I., Crandall, D., Zhang, L., Zhang, W., Irdi, G., Romanov, V., Lin, R. and Mclendon, T. R. 2016, Greenhouse Gases Science and Technology, 6, 824.
14. Davila, G., Dalton, L, Crandall, D., Garing, C., Werth, C. and Druhan, J. 2020, Geochemical et Cosmochimica Acta, 271, 227.
15. Deng, H., Fitts, J., Crandall, D., McIntyre, M. and Peters, C. 2015, Environmental Science & Technology, 49(16), 10226.
16. Wang, Y., Zhang, L., Soong, Y., Dilmore, R., Lei, H. and Li, X. 2019, Computers and Geosciences, 125, 55.
17. Deng, H., Gharasoo, M., Zhang, L., Dai, Z., Hajiadeh, A., Peters, C., Soulaine, C., Thullner, M. and Cappellen, P. 2022, Applied Geochemistry, 105445.
18. Zhang, L., Soong, Y. and Dilmore, R. 2017, Greenhouse Gases Science and Technology, 7(6), 988.
19. Szecsody, J., Zhong, L., Thomle, J., Vermeul, V., Strickland, C., Williams, M., Liu, J., McKinley, J., Bowden, J., Gilmore, M., Eisenhauer, T. and Colwell, R. 2014, Energy Procedia, 63, 3285.
20. Soong, Y., Howard, B. H., Hedges, S. W., Haljasmaa, I., Warzinski, R. P., Irdi, G. and McLendon, T. R. 2014, Aerosol and Air Quality Research, 14, 522.
21. Zhang, L., Soong, Y. and Dilmore, R. 2016, Greenhouse Gas Sci Technol., 5, 1.
22. Tutolo, B. M., Luhmann, A. J., Kong, X., Saar, M. O. and Seyfried, W. E. 2015, Geochimica et Cosmochimica Acta, 160, 132.
23. Nogurs, J. P., Fitts J. P., Celia, M. A. and Peters, C. A. 2013, Water Resour Res., 49, 6006.
24. Soong Y., Howard B., Haljasmaa I., Crandall D., Dilmore R., Dalton L., Wang, P., Tuo, J., Gray, M. and Fan, S. 2020, Tren. Chem. Eng., 18, 47.
25. Soong, Y., Howard, B., Crandall, D., Mclendon, R., Zhang, L., Lin, R., Dalton, L., Zhang, W., Fan, S. and Haljasmaa, I. 2018, Environmental Engineering Science, 35, 391.
26. Roberts-Ashby, T., Brennan, T., Merrill, D., Blondes, S., Freeman, A., Cahan, M., DeVera, A. and Lohr, D. 2012, Geologic framework for the national assessment of carbon dioxide storage resources: U.S. Geological Survey Open-File Report 1024-L, 22.
27. Roberts-Ashby, T., Stewart, M. and Ashby, B. 2013, Environment Geosciences, 20(3), 109.
28. Soong, Y., Hedges, S., Howard, B., Dilmore, R. and Allen, D. 2014, Inter. J. Energy Research, 38, 1224.
29. Cui, G., Hu, Z., Ning, F., Jiang, S. and Wang, R. 2023, Fuel, 334(1), 126615.